JPE 19-1-19

https://doi.org/10.6113/JPE.2019.19.1.201
ISSN(Print): 1598-2092 / ISSN(Online): 2093-4718

Multimode Hybrid Control Strategy of LLC Resonant Converter in Applications with Wide Input Voltage Range

Yan Li†, Kun Zhang*, and Shuaifei Yang*

†,*School of Electrical Engineering, Beijing Jiaotong University, Beijing, China

Abstract

This paper proposes a multimode hybrid control strategy that can achieve zero-voltage switching of primary switches and zero-current switching of secondary rectifier diodes in a wide input voltage range for full-bridge LLC resonant converters. When the input voltage is lower than the rated voltage, the converter operates in Mode 1 through the variable-frequency control strategy. When the input voltage is higher than the rated voltage, the converter operates in Mode 2 through the VF and phase-shift control strategy until the switching frequency reaches the upper limit. Then, the converter operates in Mode 3 through the constant-frequency and phase-shift control strategy. The secondary-side diode current will operate in the discontinuous current mode in Modes 1 and 3, whereas it will operate in the boundary current mode in Mode 2. The current RMS value and conduction loss can be reduced in Mode 2. A detailed theoretical analysis of the operation principle, the voltage gain characteristics, and the realization method is presented in this paper. Finally, a 500 W prototype with 100–200 V input voltage and 40 V output voltage is built to verify the feasibility of the multimode hybrid control strategy.

Key words: BCM, LLC resonant converter, Multimode hybrid control, Wide input voltage

I. INTRODUCTION

With the development of society and economy, renewable energy sources have been used widely in recent years. They have become more competitive than traditional energy sources. However, new energy sources have the disadvantage of a wide range of output voltages. Therefore, developing a DC/DC converter with high efficiency over a wide voltage range is necessary [1]-[3].

During last two decades, LLC resonant converter, which can realize soft switching and achieve high power density, has become a popular research subject. Normally, the LLC resonant converter operates through the variable-frequency (VF) control strategy. The operating frequency range has to be limited, which is unsuitable for applications with wide input voltage ranges [4-6]. To solve this problem, many approaches have been proposed from new topologies and control strategies.

Manuscript received Jul. 24, 2018; accepted Oct. 15, 2108
Recommended for publication by Associate Editor Fuxin Liu.
†Corresponding Author: liyan@bjtu.edu.cn
Tel: +86-10-51684911, Beijing Jiaotong University
*School of Electrical Engineering, Beijing Jiaotong University, China

In [7], a hybrid three-level (TL) LLC resonant converter capable of operating under TL and two-level modes is proposed. Although this converter integrates the advantages of two modes, which can realize high efficiency in a wide voltage range through the constant-frequency (CF) control strategy, not all the switches endure half of the input voltage under the TL mode, and two modes imply more complicated control.

A TL LLC resonant converter consisting of two half-bridges in series is proposed in [8]. When the input voltage is low, the resonant tank voltages are controlled at V_{in} and 0. When the input voltage is high, the resonant tank voltages are controlled at $V_{in}/2$ and 0. In this way, the converter can operate in a wide voltage range. However, two modes cannot realize smooth transition. At the transition point, the frequency and the DC bias voltage on the resonant capacitor can change abruptly, which can lead to unstable operation.

In [9], a modified high-efficiency LLC resonant converter with two transformers is proposed. By operating in four different modes, the normalized DC voltage gain range can be as wide as four times the minimum input voltage. However, the parameter design procedure is extremely complicated.

Besides, the various modes cannot realize smooth transition.

In [10], a hybrid control strategy based on the full-bridge (FB) LLC resonant converter is proposed. This control strategy combines the traditional VF and CF control strategies. All the switches can realize zero-voltage switching (ZVS), and the rectified diodes can achieve zero-current switching (ZCS) in a wide input voltage range. However, when the input voltage is higher, with the phase-shift angle becoming larger, the current peak value of the primary and secondary sides will increase and the converter efficiency will decrease.

This paper proposes a multimode hybrid control strategy that adopts the FB LLC resonant converter as the circuit topology. In Mode 2 with the VF and phase-shift (VF–PS) control strategy, the current flowing through the secondary diodes operates in the boundary current mode (BCM) to reduce the current RMS value and achieve only a low conduction loss. Although the input voltage increases, the converter can exhibit high efficiency.

II. Operation Principle of LLC Converter

A. VF Control

Fig. 1 shows the main circuit topology of the FB LLC resonant converter. The resonant tank is composed of L_r, L_m, and C_r. n and R_L are the transformer turns ratio and the load resistance, respectively.

In [10], when the switching frequency is lower than the resonant frequency, the VF control strategy is used. When the switching frequency is higher than the resonant frequency, the CF-PS control strategy is used to satisfy the requirements of the wide input voltage range. The hybrid control strategy can realize ZVS of the primary switches and ZCS of the secondary diodes. Although it is simple, when the input voltage is higher, the phase-shift angle can increase to reduce the voltage gain, thereby increasing the current peak value of the primary and secondary sides. Meanwhile, the primary-side circulation loss can increase, which results in low work efficiency and more difficulty for the selection of the switches and diodes.

B. VF-PS Control

In this paper, the VF-PS control strategy is proposed for the secondary-side current to operate in the BCM when the circuit works in buck mode. The main operating waveforms of the converter are shown in Fig. 2.

The figure shows eight operation stages in one switching period with the proposed control strategy, whose corresponding equivalent circuits are shown in Fig. 3. The operation is described in detail as follows.

In Stage 1 [before t_0] (Fig. 2(a)), Q_1 versus Q_2 are turned on and Q_3 versus Q_4 are turned off. During this time interval, the resonant tank voltage v_{AB} is zero, and the magnetizing inductor voltage is clamped at $-nV_o$. The converter operates in

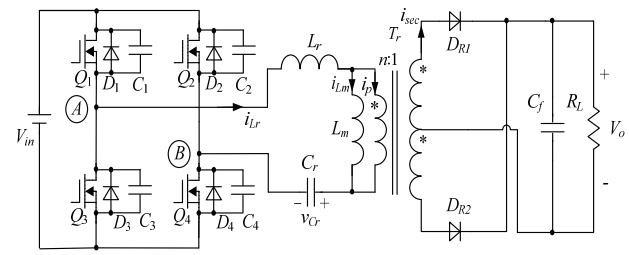

Fig. 1. FB LLC resonant converter.

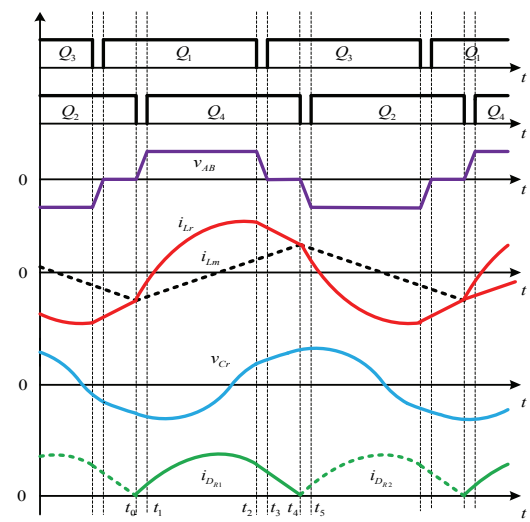

Fig. 2. Main waveforms of LLC converter with VF-PS control strategy.

this stage until the resonant current i_{Lr} is equal to the magnetizing current i_{Lm}. The rectifier diode D_{R2} is turned off, with the ZCS avoiding reverse recovery.

In Stage 2 [t_0–t_1] (Fig. 2(b)), Q_2 is turned off at t_0. During this time interval, the primary resonant current i_{Lr} begins to charge C_2 and discharge C_4 and the resonant tank voltage v_{AB} increases. This interval is short and thus can be ignored.

In Stage 3 [t_1–t_2] (Fig. 2(c)), the drain-source voltage of Q_4 decreases to 0 at t_1 while the body diode conducts, thereby ensuring that the ZVS turn-on of switch Q_4 can be achieved subsequently. The magnetizing inductor voltage is clamped at nV_o, and the magnetizing current i_{Lm} increases linearly. The resonant tank voltage v_{AB} is equal to V_{in}. The primary resonant current i_{Lr} is sinusoidal due to the resonance between L_r and C_r, and the rectifier diode D_{R1} is conducting at the same time. The resonant current i_{Lr}, the magnetizing current i_{Lm} and the resonant capacitor voltage v_{Cr} can be expressed as follows:

$$i_{Lr}(t) = -I_m \cos\omega_r(t-t_1) + ((V_{in} - nV_o) - V_{Cr}(t_1))\frac{1}{Z_0}\sin\omega_r(t-t_1), \tag{1a}$$

$$v_{Cr}(t) = -I_m Z_0 \sin\omega_r(t-t_1) + (V_{in} - nV_o) - [(V_{in} - nV_o) - V_{Cr}(t_1)]\cdot\cos\omega_r(t-t_1), \tag{1b}$$

$$i_{Lm}(t) = \frac{nV_o}{L_m}(t-t_1) - I_m . \tag{1c}$$

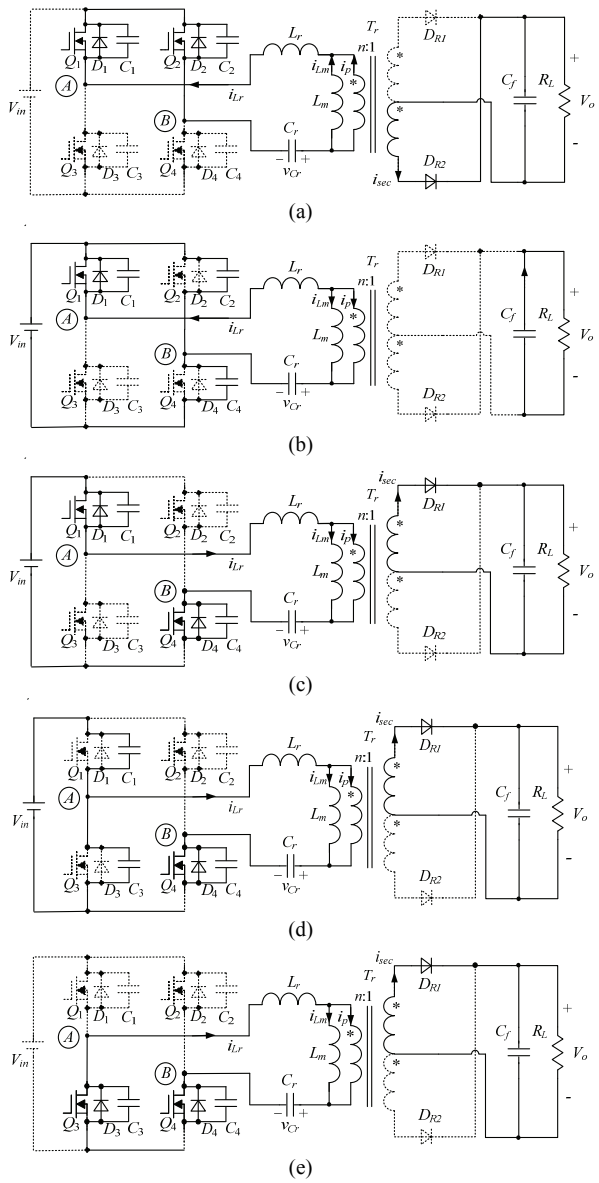

Fig. 3. Equivalent circuit with VF-PS control strategy: (a) Stage 1; (b) Stage 2; (c) Stage 3; (d) Stage 4; (e) Stage 5.

where $\omega_r = 1/\sqrt{L_r C_r}$ is the resonance angular frequency, $Z_0 = \sqrt{L_r/C_r}$ is the characteristic impedance, and I_m is the magnetizing current.

In Stage 4 [t_2–t_3] (Fig. 2(d)), Q_1 is turned off at t_2 while the resonant current i_{Lr} begins to charge C_1 and discharge C_3. And the resonant tank voltage v_{AB} starts to decrease from V_{in}. This interval is short and can thus be ignored.

In stage 5 [t_3–t_4] (Fig. 2(e)), the drain-source voltage of Q_3 decreases to 0 and the body diode conducts simultaneously, thereby ensuring that the ZVS turn on of switch Q_3 can be achieved subsequently. Meanwhile, the resonant tank voltage v_{AB} is zero, and the magnetizing inductor voltage is clamped at nV_o. The resonant current i_L, the magnetizing current i_{Lm} and the resonant capacitor voltage v_{Cr} can be expressed as follows.

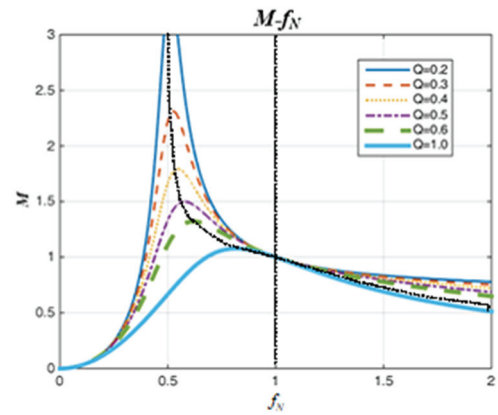

Fig. 4. Gain curves in VF control strategy.

$$i_{Lr}(t) = I_{Lr}(t_3)\cos\omega_r(t-t_3) + [-nV_o - V_{Cr}(t_3)]\cdot \frac{1}{Z_0}\sin\omega_r(t-t_3), \tag{2a}$$

$$v_{Cr}(t) = I_{Lr}(t_3)Z_0\sin\omega_r(t-t_3) + (-nV_o) - [-nV_o - V_{Cr}(t_3)]\cdot\cos\omega_r(t-t_3), \tag{2b}$$

$$i_{Lm}(t) = \frac{nV_o}{L_m}(t-t_1) - I_m. \tag{2c}$$

The next five operation stages are similar to the former five, then a new period begins.

Fig. 2 shows that the rectifier diode current operates in BCM when $\omega_r t_4 = \pi$.

III. Voltage Gain Characteristic

A. Voltage Gain Analysis in VF Control

As the switching frequency f_s varies closer to the resonant frequency f_r with the VF control strategy, the fundamental harmonic approximation (FHA) method is used to obtain the voltage gain characteristics [11]-[16]. The specific derivation process is no longer described.

Fig. 4 shows the voltage gain characteristic when $\lambda = 3$, where λ is the ratio of the magnetizing inductance L_m to the resonant inductance L_r. When the switching frequency is lower than the resonant frequency, the converter operates in boost mode, and when the switching frequency is higher than the resonant frequency, the converter operates in buck mode. Eq. 3 shows the voltage gain expression where Q is the quality factor and f_N is the normalized frequency.

$$M = \frac{1}{\sqrt{\left[\left(1-\frac{1}{(f_N)^2}\right)Qf_N\right]^2 + \left[\left(1-\frac{1}{(f_N)^2}\right)\frac{1}{\lambda}+1\right]^2}}. \tag{3}$$

B. Voltage Gain Analysis in VF-PS Control

FHA analysis is no longer applicable to the VF-PS control strategy. Therefore, the time-domain analysis method is used to obtain the voltage gain characteristics.

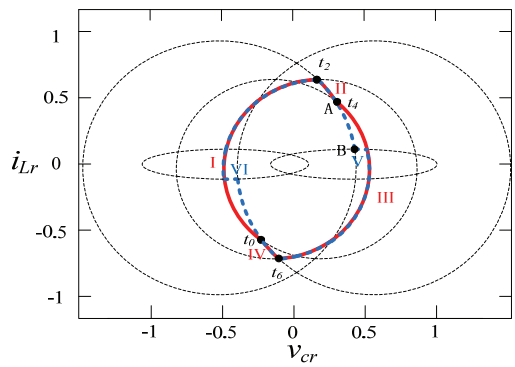

Fig. 5. Steady-state trajectory for the hybrid control strategy.

To simplify the analysis, $V_{base} = V_{in}$, $\omega_{base} = \omega_r$, $R_{base} = Z_0$, and $I_{base} = V_{in}/Z_0$ can be chosen to obtain normalized variables [7]. Then, $\theta = \omega_r t$ and $D_y = T_{on}/(T_s/2)$ are defined, where T_s represents the switching period and T_{on} represents the time when Q_1 and Q_4 or Q_2 and Q_3 are on. The relationship between t and θ can be expressed by

$$\theta_0 = \omega_r t_0 = 0\,, \tag{4a}$$

$$\theta_1 = \omega_r t_2 = \omega_r D_y T_s / 2 = D_y \pi / f_N\,, \tag{4b}$$

$$\theta_2 = \omega_r t_4 = \omega_r T_s / 2 = \pi / f_N\,. \tag{4c}$$

According to Eqs. 1 and 2, normalized equations can be obtained as follows.

When $0 \le \theta \le \theta_1$,

$$\begin{cases} i_{Lr}^*(\theta) = -I_m^* \cos\theta + (1 - M - V_{cr}^*(0)) \cdot \sin\theta \\ v_{cr}^*(\theta) = -I_m^* \sin\theta - (1 - M - V_{cr}^*(0)) \cdot \cos\theta \\ \qquad\qquad + (1 - M) \\ i_{Lm}^*(\theta) = -I_m^* + M\theta / \lambda \end{cases}. \tag{5}$$

When $\theta_1 \le \theta \le \theta_2$,

$$\begin{cases} i_{Lr}^*(\theta) = I_{Lr}^*(\theta_1)\cos(\theta - \theta_1) + (-M - V_{cr}^*(\theta_1)) \cdot \\ \qquad\qquad \sin(\theta - \theta_1) \\ v_{cr}^*(\theta) = I_{Lr}^*(\theta_1)\sin(\theta - \theta_1) - (-M - V_{cr}^*(\theta_1)) \\ \qquad\qquad \cdot\cos(\theta - \theta_1) - M \\ i_{Lm}^*(\theta) = -I_m^* + M\theta / \lambda \end{cases}. \tag{6}$$

Fig. 5 shows the trajectory when the normalized resonant current and the resonant capacitor voltage are mapped to the state plane. With the dead time ignored, the start transient of each stage is shown in Fig. 5. The blue dotted line is the traditional CF-PS control strategy. The circle centers of stages V and VI are (0.5, 0) and (-0.5, 0), respectively. The red solid line is the VF-PS control strategy, which includes four different stages. The circle centers of stages I to IV are (1-M,0), (-M,0), (M-1,0), and (M,0). Stages I and III represent the stages v_{AB} equals V_{in}. Stages II and IV represent the stages v_{AB} equals 0.

According to Fig. 5, the transition point between Stages II and III is at A(t_4) with the VF-PS control strategy, and the transition point between Stages II and V is at B with the CF-PS control strategy. Therefore, completing the switch transition at point A is the necessary and sufficient condition for the secondary-side diode current to realize BCM.

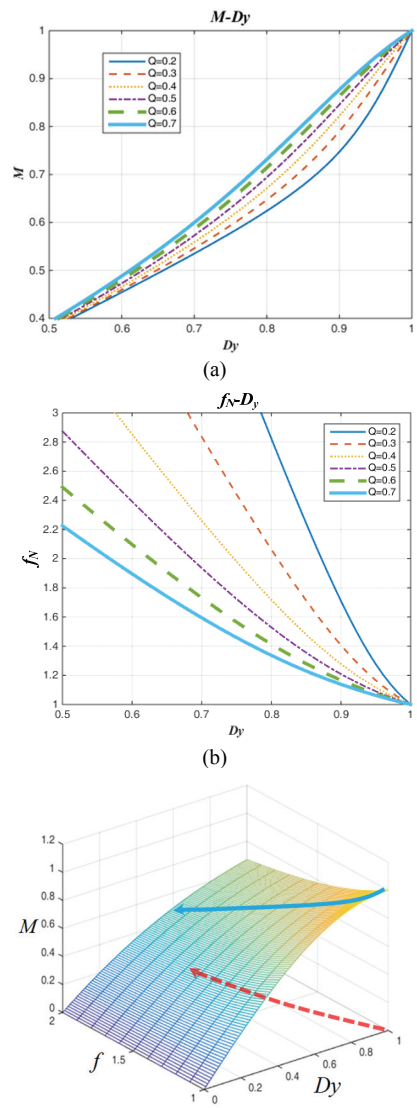

Fig. 6. Curves of gain versus duty ratio and frequency versus duty ratio for VF-PS control strategy: (a) M-D_y curves; (b) f-D_y curves; (c) 3D graph of f, D_y and M.

According to the symmetry of Fig. 2, the boundary conditions can be obtained as follows:

$$I_{Lr}^*(\theta_2) = I_{Lm}^*\,, \tag{7}$$

$$I_{Lm}^*(\theta_2) = I_m^*\,, \tag{8}$$

$$V_{cr}^*(\theta_2) = -V_{cr}^*(0)\,. \tag{9}$$

Furthermore, the load current can be expressed as

$$\begin{aligned} I_o &= \frac{1}{T_s/2}\int_{t_0}^{t_4} i_{\sec}(t)dt \\ &= n\frac{1}{T_s/2}\int_{t_0}^{t_4}(i_{Lr}(t) - i_{Lm}(t))dt \end{aligned}. \tag{10}$$

From t_0 to t_4, the integral of the resonant current over time

is the charged charge of the resonant capacitor. Thus,

$$V_{cr}^{*}(\theta_2)-V_{cr}^{*}(\theta_0)=\frac{8Q}{\pi^2}\theta_2 M \ . \tag{11}$$

According to Eqs. (5)–(11),

$$\begin{gathered}-(1+\cos\theta_2)\cdot I_{\mathrm{m}}^{*}-\sin\theta_2\cdot V_{cr}^{*}(0)-\sin\theta_2\cdot M+\\ \sin\theta_2-\sin(\theta_2-\theta_1)=0\end{gathered}, \tag{12}$$

$$\begin{gathered}-\sin\theta_2\cdot I_{\mathrm{m}}^{*}+(1+\cos\theta_2)\cdot V_{cr}^{*}(0)+\\ (\cos\theta_2-1)\cdot M+\cos(\theta_2-\theta_1)-\cos\theta_2=0\end{gathered}, \tag{13}$$

$$\begin{gathered}-\sin\theta_2\cdot I_{\mathrm{m}}^{*}+(\cos\theta_2-1)\cdot V_{cr}^{*}(0)+\\ (\cos\theta_2-1-\frac{8\theta_2 Q}{\pi^2})\cdot M+\cos(\theta_2-\theta_1)-\cos\theta_2=0\end{gathered}. \tag{14}$$

As shown in the above equations, the parameters are θ_1, θ_2, M, I_m^*, V_{Cr}^*, Q, and λ. Some of them can be expressed by λ = 3, $\theta_1 = D_y\pi/f_N$, $\theta_2 = \pi/f_N$, and $I_m^* = M\theta_2/2\lambda$, where Q depends on the load. Therefore, the equations can be solved by using the software MATLAB. When Q and λ are determined, the curves of gain versus duty ratio and frequency versus duty ratio for the VF-PS control strategy can be obtained as shown in Fig. 6. Given that the converter can maintain high efficiency when the duty ratio is more than 0.5, Figs. 6(a) and 6(b) show only the duty ratio between 0.5 and 1.

Fig. 6(c) shows that when the load is constant, a unique relationship between f_N and D exists to satisfy the different gain requirements. Therefore, the frequency and duty ratio can be changed simultaneously to reduce the voltage gain.

On the basis of the above analysis, the output voltage of the LLC resonant converter can be adjusted by the frequency and duty ratio. In this paper, the VF-PS control strategy is used to find the optimal curve on the plane for the secondary-side diode current to operate in BCM.

IV. Multimode Hybrid Control Strategy

Fig. 7 shows the traditional hybrid control strategy. When the switching frequency is lower than the resonant frequency, the converter operates in Mode 1 with the VF control strategy. When the switching frequency is higher than the resonant frequency, the converter operates in Mode 2 with the CF-PS control strategy.

In this paper, a multimode hybrid control strategy is proposed by combining the advantages of the VF and VF-PS control strategies. When the input voltage is below the rated voltage, the converter operates in Mode 1 with the VF control strategy. When the input voltage is above the rated voltage, the converter operates in Mode 2 with the VF-PS control strategy until the switching frequency reaches the upper limit frequency, which is equal to 2.4 fr. Then, the switching frequency remains constant, and the converter begins to operate in Mode 3. This mode prevents the switching frequency variation range from being excessively wide. The control diagram and gain curves are as shown in Figs. 8 and 9, respectively.

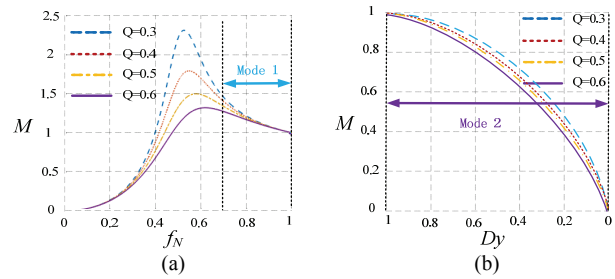

Fig. 7. Gain curves of traditional hybrid control strategy: (a) Mode 1; (b) Mode 2.

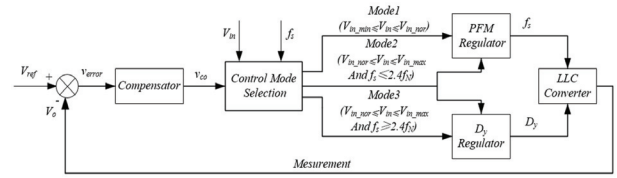

Fig. 8. Control diagram of multimode control strategy.

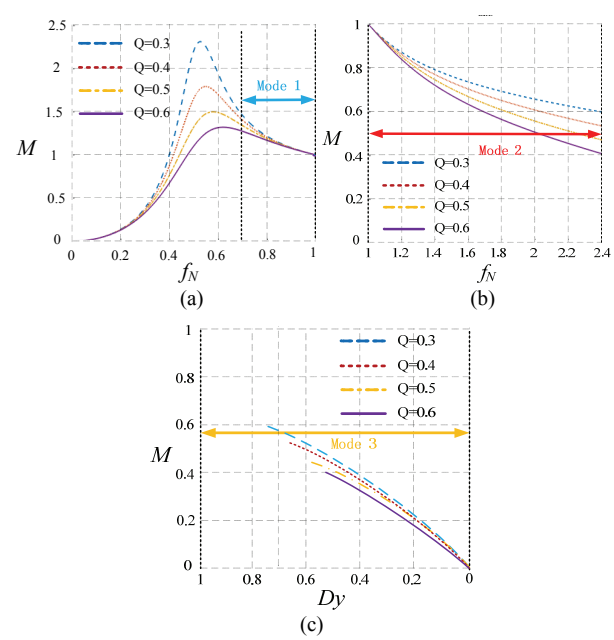

Fig. 9. Gain curves of multimode hybrid control strategy: (a) Mode 1; (b) Mode 2; (c) Mode 3.

V. Analysis of the Curret Peak Value

The conduction loss of the LLC converter is related to the current value of the primary side. To simplify the analysis, the resonant current operating stages of a switching period are reclassified. Through the analysis, the primary-side current peak equations can be obtained.

Fig. 10 shows the main operating waveforms of the current in boost mode with the VF control strategy. The area switching period has four operation stages.

In Stage 1 [0-T_r/2], the resonant inductance and resonant capacitor participate in the resonance. The resonant current i_{Lr} and the magnetizing current i_{Lm} can be expressed by

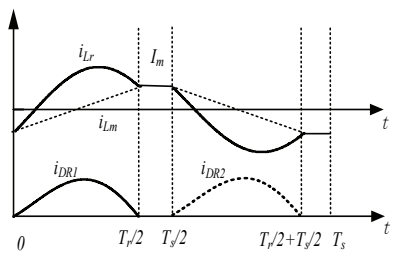

Fig. 10. Waveforms i_{Lr} and i_{DR1} of LLC converter with VF control strategy.

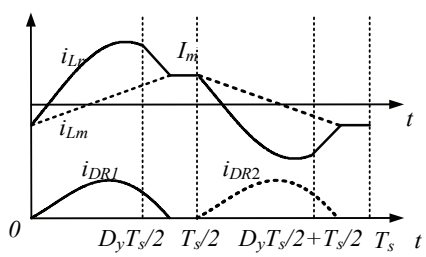

Fig. 11. Waveforms i_{Lr} and i_{DR1} of LLC converter with CF-PS control strategy.

$$i_{Lr}(t) = I_{Lr\_peak}\sin(\omega t + \psi), \tag{15}$$

$$i_{Lm}(t) = \frac{nV_o}{L_m}t - I_m, \tag{16}$$

where I_{Lr_peak} is the current peak value of the resonant network and ψ is the initial phase angle.

In Stage 2 [$T_r/2$-$T_s/2$], the resonant inductor, the resonant capacitor, and the magnetizing inductor participate in the resonance. The resonant current i_{Lr} equals the magnetizing current i_{Lm}.

During half of the resonance period, the primary-side transmits energy to the secondary-side. Hence,

$$\int_0^{\frac{T_r}{2}} nV_o\left[i_{Lr}(t) - i_{Lm}(t)\right]dt = \frac{V_o^2}{R_L}\frac{T_s}{2}. \tag{17}$$

According to Eqs. (15)–(17), the resonant current peak value can be expressed as

$$I_{Lr\_peak} = \frac{V_o}{2n}\sqrt{\frac{n^4}{4L_m^2 f_r^2} + \frac{\pi^2}{R_L^2}\left(\frac{f_r}{f_s}\right)^2}. \tag{18}$$

Fig. 11 shows the main operating waveforms of the current in buck mode with use of the traditional CF-PS control strategy. The current peak value can be expressed by using similar methods.

$$I_{Lr\_peak} = \sqrt{\left(\frac{D_y nV_o}{4L_m f_s}\right)^2 + \left(\frac{\pi V_o}{2nD_y R_L}\right)^2} \tag{19}$$

Fig. 12 shows the main operating waveforms of the current in buck mode with use of the VF-PS control strategy.

When t is between 0 and $D_yT_s/2$, the resonant current i_{Lr} and the magnetizing current i_{Lm} can be expressed by Eqs. 15 and 16 similarly. However, the angular frequency ω is slightly different.

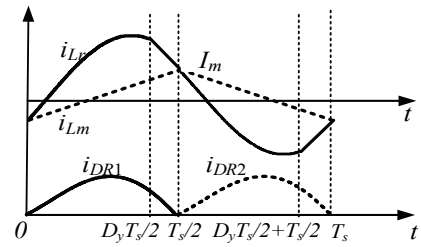

Fig. 12. Waveforms i_{Lr} and i_{DR1} of LLC converter with VF-PS control strategy.

TABLE I
KEY CIRCUIT PARAMETERS

Parameters	Values
Rated input voltage	120 V
Input voltage range	100–200 V
Resonant frequency (fr)	50 kHz
Magnetizing inductance (Lm)	$129\mu H$
Resonant inductance (Lr)	$43\mu H$
Resonant capacitor (Cr)	$253nF$

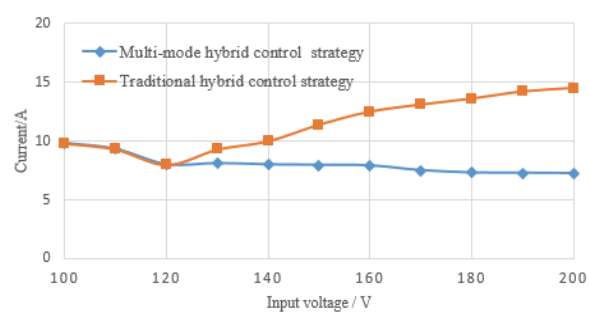

Fig. 13. Primary-side current peak value with different control strategies.

During the stage, the primary side transmits energy to the secondary side. Hence,

$$\int_0^{\frac{D_yT_s}{2}} nV_o\left[i_{Lr}(t) - i_{Lm}(t)\right]dt = \frac{V_o^2}{R_L}\frac{D_yT_s}{2}. \tag{20}$$

Finally, the resonant current peak with the VF-PS control strategy can be expressed as

$$I_{Lr\_peak} = \sqrt{\left(\frac{nV_o}{4L_m f_s}\right)^2 + \left(\frac{\pi V_o}{2nR_L} - \frac{\pi(1-D_y)nV_o}{8L_m f_s}\right)^2}. \tag{21}$$

To illustrate the advantages of the proposed multimode hybrid control strategy, a 500 W power prototype with 100-200 V input voltage and 40 V output voltage is built. The detailed parameters are presented in Table I.

According to the current peak value equations under different control strategies and Table I, the primary-side current peak curves at different input voltages can be obtained as shown in Fig. 13.

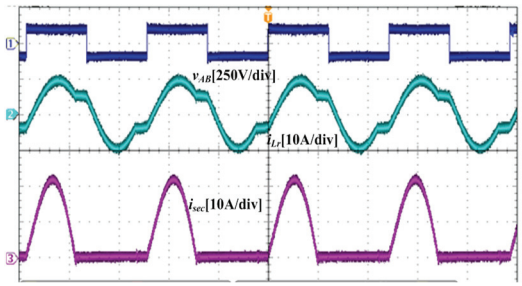

Fig. 14. Waveforms with input voltage Vin = 100 V.

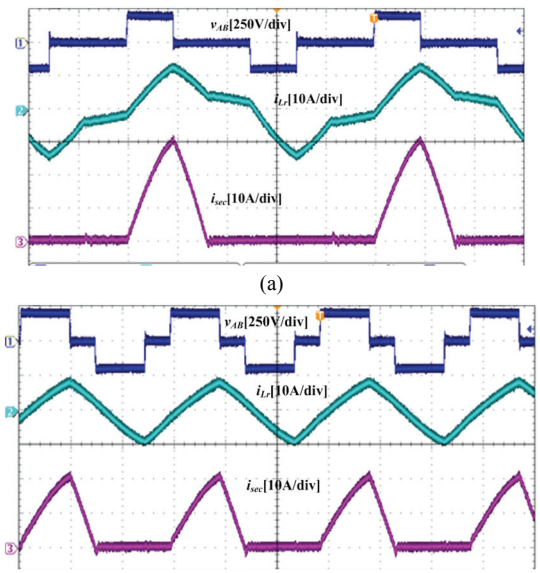

(a)

(b)

Fig. 15. Waveforms with input voltage Vin = 200 V: (a) CF-PS control strategy; (b) VF-PS control strategy.

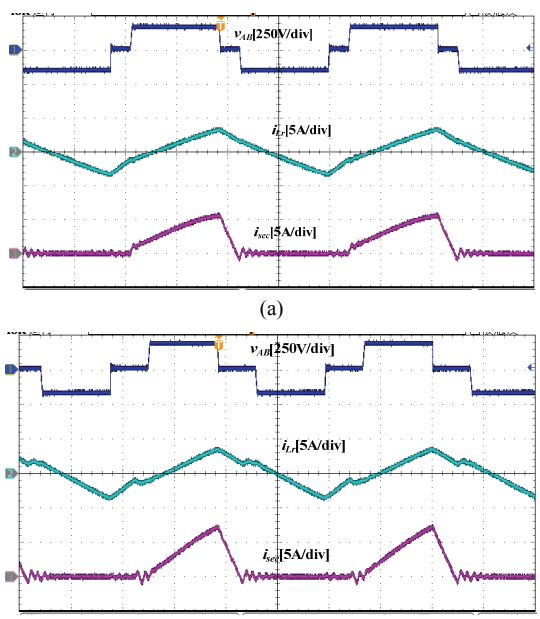

(a)

(b)

Fig. 16. Waveforms with different input voltages at 30% load: (a) Vin = 160 V; (b) Vin = 180 V.

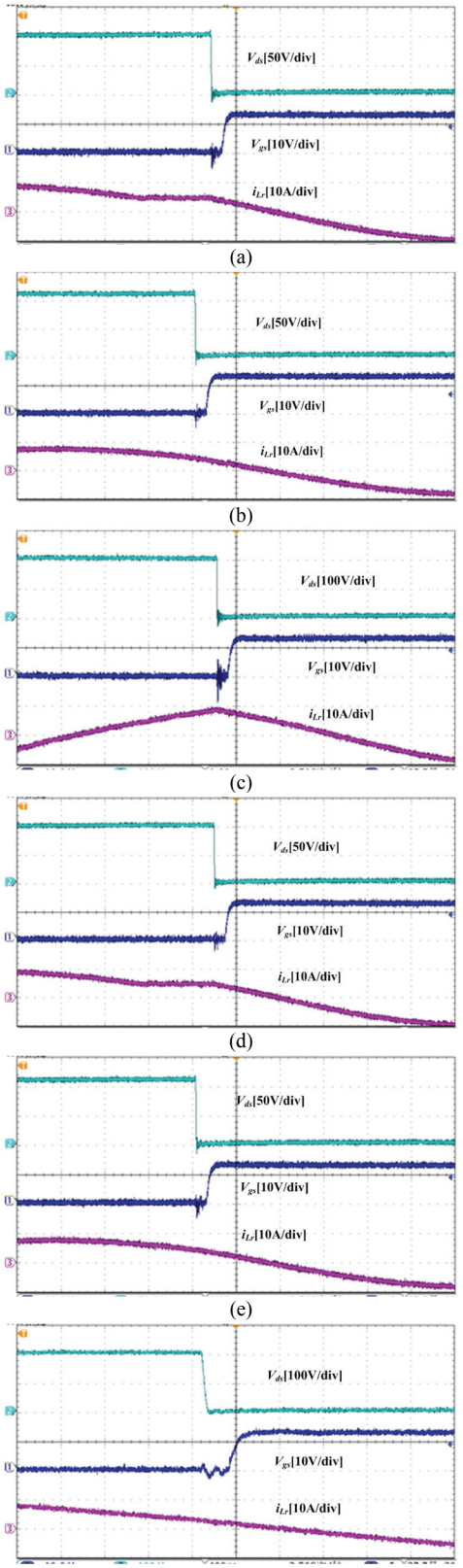

(a)

(b)

(c)

(d)

(e)

(f)

Fig. 17. ZVS waveforms of switches Q_2 and Q_3 with the converter operating at full load: (a) Vin = 100 V, waveforms of Q_3; (b) Vin = 120 V, waveforms of Q_3; (c) Vin = 200 V, waveforms of Q_3; (d) Vin = 100 V, waveforms of Q_2; (e) Vin = 120 V, waveforms of Q_2; (d) Vin = 200 V, waveforms of Q_2.

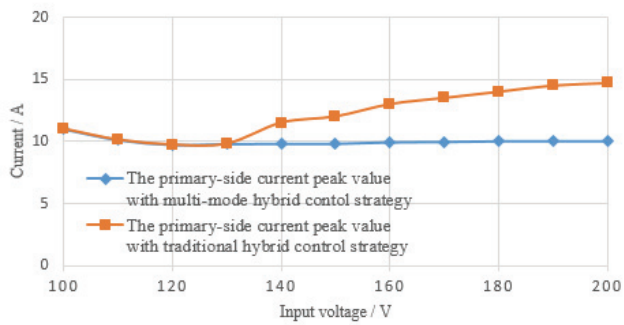

Fig. 18. Primary-side and secondary-side current peak values with different control strategies.

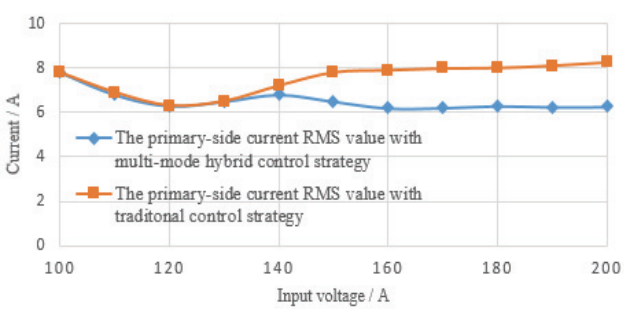

Fig. 19. Primary-side current RMS value with different control strategies.

As shown in the figure, the resonant current peak value of the VF-PS control strategy is lower than that of the CF-PS control strategy. Therefore, the conduction loss can be reduced in buck mode by the VF-PS control strategy, which is beneficial to the selection of switches and diodes.

VI. Experimental Results

In this paper, the 120 V input voltage is set as the transition point between Mode 1 and Mode 2, and the point at $f_r = f_s$ and $M = 1$. The upper limit frequency is set to 2.4 times f_r as the transition point between Mode 2 and Mode 3.

Fig. 14 shows the waveforms when the input voltage is 100 V at full load with the VF control strategy. Fig. 15 shows the waveforms when the input voltage is 200 V at full load with the traditional CF-PS control strategy and the proposed VF-PS control strategy. The waveforms when the converter operates at 30% load are shown in Fig. 16.

As shown in Fig. 16, when the input voltage is 160 V, the converter operates in Mode 2, and when the input voltage is 180 V, the converter reaches the upper limit frequency and operates in Mode 3. Fig. 17 shows the soft switching waveforms of switches Q_2 and Q_3 at different input voltages when the converter operates at full load.

Fig. 18 shows the primary-side and secondary-side current peak values with different hybrid control strategies, and Fig. 19 shows the primary-side current RMS value with different hybrid control strategies.

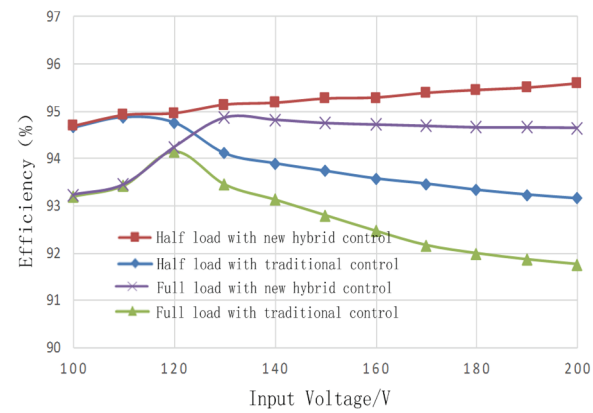

(a)

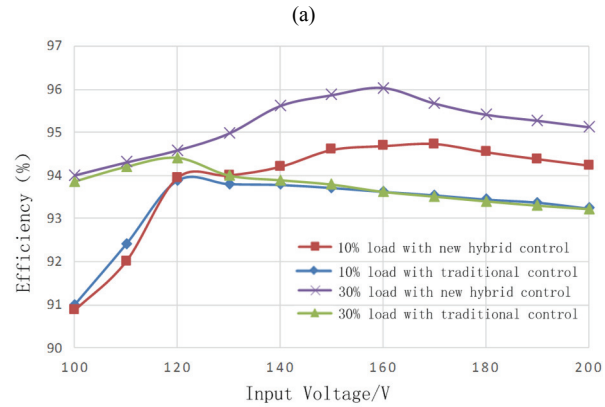

(b)

Fig. 20. Efficiency of the converter with different control strategies: (a) Full load and half load; (b) 10% and 30% load.

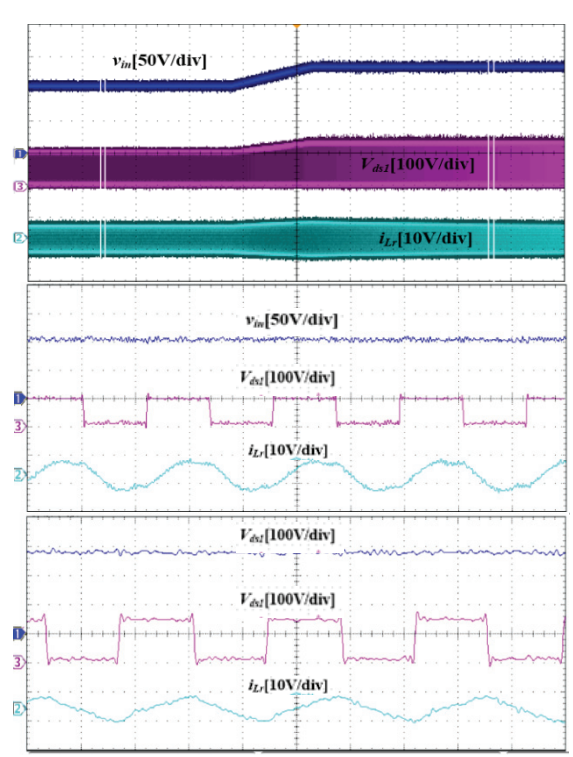

Fig. 21. Experimental waveforms of transition between Mode 1 and Mode 2.

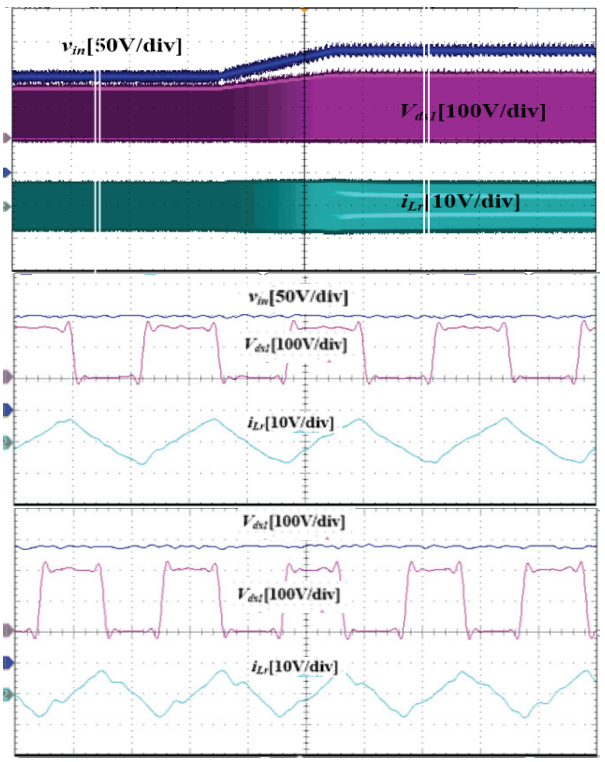

Fig. 22. Experimental waveforms of mode transition between Mode 2 and Mode 3.

As can be seen in Figs. 13 and 18, the theoretically and experimentally simulated curves agree well.

According to Fig. 19, the primary-side current RMS value with the multimode hybrid control strategy is less than that with the traditional hybrid control strategy when the input voltage increases at full load. Meanwhile, the secondary-side diode current operates in BCM when the converter operates in Mode 2.

When the converter operates in Mode 2, the switching frequency increases with the input voltage. The conduction and circulation losses can thus be reduced. Therefore, the converter can achieve high efficiency. Fig. 20 shows the efficiency of the converter with the control strategies at different loads.

Fig. 21 shows the transition from Mode 1 to Mode 2 when the input voltage changes from 100 V to 140 V at half load. Fig. 22 shows the transition from Mode 2 to Mode 3 when the input voltage changes from 150 V to 190 V at 30% load. The experimental waveforms show that smooth transitions between different modes can be easily achieved.

VII. Conclusion

This paper proposes a multimode hybrid control strategy that is based on the FB LLC resonant converter. All primary-side switches operate with the ZVS, and the secondary-side diodes turn off with the ZCS in a wide input voltage and full-load range. Three operating modes are used to adjust the output voltage in a wide input voltage range. The secondary-side diode current operates in DCM in Modes 1 and 3. However, it operates in BCM in Mode 2. Hence, the circulation losses and the current peak value in the primary and secondary sides can be reduced, and high efficiency can be realized. The performance of the proposed hybrid control strategy is experimentally verified by a 500 W power converter prototype with 100–200 V input voltage and 40 V output voltage. Therefore, the FB LLC resonant converter with the multimode hybrid control strategy is a good candidate for applications with wide input voltage ranges.

Acknowledgment

This work was supported by the Lite-On Power Electronics Technology Research Fund under Grant No. PRC20170952.

References

[1] F. Q. Bo and J. F. Shen, "Z-source resonant DC-DC converter for wide input voltage," *Techniques of Automation & Applications*, Vol. 32, No. 10, pp. 46-55, Oct. 2013.

[2] S. L. Du, X. Y. Jia, C. S. Hu, and D. H. Xu, "Characterization of phase shift control of LLC resonant converter," *Power Electronics*, Vol. 50, No. 9, pp. 51-53, Sep. 2016.

[3] T. LaBella, W. S. Yu , J.S Lai , M. Senesky, and D. Anderson, "A bidirectional-switch-based wide-input range high-efficiency isolated resonant converter for photovoltaic applications," *IEEE Trans. Power Electron.*, Vol. 29. No. 7, pp. 3473-3484, Jul. 2014.

[4] D. K. Kim, S. C. Moon, C. O Yeon, and G. W. Moon, "High-efficiency LLC resonant converter with high voltage gain using an auxiliary LC resonant circuit," *IEEE Trans. Power Electron.*, Vol. 31, No. 10, pp. 6901-6909, Oct. 2016.

[5] Y. Zhang, J. L. Shi, and L. Zhou, "Wide input-voltage range boost three-level DC-DC converter with quasi-Z source for fuel cell vehicles," *IEEE Trans. Power Electron.*, Vol. 32, No. 9, pp. 6728-6738, Sep. 2017.

[6] P. P. Meng, X. Wu, C. Zhao, J. Zhang, and Z. Qian, "A novel variable frequency soft switching full-bridge DC/DC converter with critical continuous mode control," *Proceedings of the CSEE*, Vol. 32, No. 6, pp. 106-112, Feb. 2012.

[7] K. Jin and X. B. Ruan, "Hybrid full bridge three-level LLC resonant converter," *Proceedings of the CSEE*, Vol. 26, No. 3, pp. 53-58, Jan. 2006.

[8] H. Y. Li, W. Zhen, L. Zhao, and J. H. Zhang, "Multi-level control strategy of wide input LLC resonant converter," *Trans. China Electrotechnical Soc.*, Vol. 32, No. 4, pp. 48-57, Feb. 2017.

[9] H. Hu, X. Fang, F. Chen, Z. J. Shen, and I. Batareh, "A

modified high-efficiency LLC converter with two transformers for wide input-voltage range application," *IEEE Trans Power Electron*, Vol. 28, No. 4, pp. 1946-1960, Apr. 2013.

[10] J. Li and X. B. Ruan, "Research on the hybrid control strategy of full bridge LLC converter," *Trans. China Electrotechnical Soc.*, Vol. 28, No. 4, pp. 72-80, Mar. 2013.

[11] J. W. Zhang and F. D. Zhou, "A full-bridge LLC voltage-multiplying resonant converter base on phase-shifted control," *Power Electronics*, Vol. 47, No. 5, pp. 94-103, May. 2013.

[12] F. C. Lee, "High-frequency quasi-resonant converter technologies," *Proc. IEEE*, Vol. 76, No. 4, pp.377-390, Apr. 1988.

[13] X. Ruan, Z. Chen, and W. Chen, "Zero-voltage-switching PWM hybrid full-bridge three-level converter," *IEEE Trans. Power Electron.*, Vol. 20, No. 2, pp. 395-404, Feb. 2005.

[14] L.Shi, B.P. Baddipadiga, M. Ferdowsi, and M. L. Crow, "Improving the dynamic response of a flying-capacitor three-level Buck converter," *IEEE Tran. Power Electron.*, Vol. 28, No. 5, pp. 2356-2365, May. 2013.

[15] G. Ivensky, S. Bronshtein, and A. Abramovitz, "Approximate analysis of resonant LLC DC-DC converter," *IEEE Trans. Power Electron.*, Vol. 26, No. 11, pp. 3274-3284, Apr. 2011.

[16] Q. C. Chen, Y. C. Ji, and J. Z. Wang, "Analysis and design of bidirectional CLLLC resonant DC-DC transformers," *Proc. CSEE*, Vol.34, No. 18, pp. 2898-2905, Jun. 2014.

Yan Li was born in Heilongjiang Province, China, in 1977. She received the B.S. and M.S. degrees in electrical engineering from Yanshan University, Qinhuangdao, China, in 1999 and 2003, respectively, and her Ph.D. degree in electrical engineering from the Nanjing University of Aeronautics and Astronautics, Nanjing, China, in 2009. From 1999 to 2009, she was at Yanshan University, Hebei, China. Since 2009, she has been in the School of Electrical Engineering, Beijing Jiaotong University, Beijing, China. Her current research interests include multiple-input dc/dc converters, renewable power systems, and PV grid-tied systems.

Kun Zhang was born in Shanxi Province, China, in 1992. He received the B.S. and M.S. degrees in electrical engineering from Beijing Jiaotong University, Beijing, China, in 2015 and 2018, respectively. His research interests include wide-input dc/dc converters and renewable power systems.

Shuaifei Yang was born in Henan Province, China, in 1996. He received the B.S. degree in electrical engineering from Tianjin University of Science and Technology, Tianjin, China, in 2018. He is currently pursuing a M.S. degree in electrical engineering at Beijing Jiaotong University. His research interests include circuits and control of wide-input dc/dc converters.